Microscopic Theory of Second Harmonic Generation at Si(100) Surfaces

Bernardo S. Mendoza,[1,2,*] Andrea Gaggiotti,[2] and Rodolfo Del Sole[2]
[1]*Centro de Investigaciones en Optica, A. C., León, Guanajuato, México*
[2]*Istituto Nazionale per la Fisica della Materia-Dipartimento di Fisica, II Università di Roma Tor Vergata, Rome, Italy*
(Received 13 May 1998)

We apply a microscopic formulation to calculate the second harmonic spectra of clean and hydrogenated Si(100) surfaces. We find a trend of the surface-allowed E_1 resonance as a function of the hydrogen coverage, which is consistent with experiment. Another resonance at lower energy, recently observed at the clean surface, is also reproduced and explained in terms of transitions across surface states. Its quenching is clearly demonstrated as a function of hydrogen coverage. Our results for the energetically more favorable $c(4 \times 2)$ structure are in better agreement with low temperature experimental data than those calculated for the 2×1 reconstruction. We find that the spectra are dominated by the $\chi^s_{\parallel\parallel\perp}$ component of the second-order nonlinear surface susceptibility. [S0031-9007(98)07375-X]

PACS numbers: 78.66.–w, 42.65.An, 42.65.Ky

The recently developed high-power tunable laser systems have opened the possibility of using nonlinear optical spectroscopies for the study of surface physics, as they have a high-surface sensitivity, are noninvasive, and are nondestructive. They can be used out of UHV conditions and even at buried interfaces [1]. In particular, the surface sensitivity of second harmonic generation (SHG) from centrosymmetric materials originates from the fact that it is forbidden, within the dipole approximation, in the bulk, due to the inversion symmetry, so that only the surface can radiate. Daum *et al.* [2] have shown that the bulk E_1 transition of Si yields a SHG resonance at the (100), clean or oxide covered, surface. This was attributed to the strain induced by the surface reconstruction in the first monolayers; it was also shown that the absorption of hydrogen quenches the resonance, probably because it relieves the surface stress. A theoretical model by Mendoza and Mochán [3], based on the phenomenological polarizable-bond description of the surface local-field effect, supported this conclusion. This SHG resonance has been used by several groups to study different aspects of the Si (100) and (111) surfaces with different reconstructions, adatom coverage, etc. [4,5]. Recently, Höfer [6] and Dadap *et al.* [7] have done a comprehensive experimental study of the clean and hydrogen-covered Si(100) double-domain surface as a function of hydrogen coverage and temperature. They demonstrate the ability of SHG to describe the dynamics of hydrogen adsorption on this surface, and that the quenching of the E_1 resonance as a function of hydrogen coverage is not as strong as that found by Daum *et al.* [2]. These experiments show how SHG spectroscopy is becoming a reliable surface tool, and thus the need of microscopic models to understand the underlying physics.

In this Letter we present a microscopic calculation of surface SHG from clean and hydrogen-covered Si(100) surfaces, which, besides giving an excellent agreement with experiments, sheds light on nonlinear optical phenomena at semiconductor surfaces. We show that the bulk E_1 resonance occurs in surface SHG spectra through electronic transitions across surface-perturbed bulk states, that hydrogen adsorption modifies the SHG line shape by reducing the E_1 resonance and suppressing the spectral structures due to transitions across surface states, and that, contrary to what may be argued, the $\chi^s_{\perp\perp\perp}$ component of the second-order surface susceptibility does not dominate the SHG signal. We find that the $\chi^s_{\parallel\parallel\perp}$ component of the second-order surface susceptibility is mostly responsible for the observed features. Therefore, it is the interplay of both in-plane and perpendicular components of $\overleftrightarrow{\chi}^s$ that gives rise to the SH response.

We calculate the reflected SHG efficiency $\mathcal{R}$ through the second-order surface susceptibility tensor $\overleftrightarrow{\chi}^s$. For an isotropic surface, such as the double-domain Si(100) surface considered here, the p-polarized SH output is given by

$$\mathcal{R}_{pi} = \frac{32\pi^3}{(n_0 e)^2 c^3}\, \omega^2 \tan^2\theta |T_p(2\omega) T_i^2(\omega) r_{pi}|^2, \qquad (1)$$

where $i = s$ or p indicates the polarization of the incoming photon of frequency ω. Here,

$$r_{pp} = \sin^2\theta\, \chi^s_{\perp\perp\perp} + (c/\omega)^2 k_\perp^2(\omega)\, \chi^s_{\perp\parallel\parallel} - (c/\omega)^2 k_\perp(\omega) k_\perp(2\omega)\, \chi^s_{\parallel\parallel\perp}, \qquad (2)$$

and $r_{ps} = \chi^s_{\perp\parallel\parallel}$. The s-polarized SH is identically zero due to symmetry considerations. Also, θ is the angle of incidence, c the speed of light, e the electron charge, n_0 the electron density of the system, T_i the transmission Fresnel factor for the i polarization, and $k_\perp = (\omega/c)[\epsilon(\omega) - \sin^2\theta]^{1/2}$, $\epsilon(\omega)$ being the bulk dielectric function. We notice that all components of $\overleftrightarrow{\chi}^s$ different from zero contribute to $\mathcal{R}_{pp}$. These expressions are strictly valid within the dipole approximation. Nevertheless, even if quadrupolar corrections are considered, the isotropic and anisotropic bulk quadrupole terms in $\mathcal{R}$ have been shown to yield negligible contributions as compared to the surface dipole terms [3,8].

The key ingredient of the calculation is $\overleftrightarrow{\chi}^s$. Following Ref. [9], we briefly sketch the procedure taken to calculate it. We model the semi-infinite crystal by a slab. The imaginary part of the single-domain second-order surface susceptibility is given by

$$\chi^{II}_{ijk}(\omega) = \frac{\pi n_0 e^4}{2Am^3\omega^3} \sum_{\vec{k}} \sum_{r\in C} \sum_{s\in V} \times \left\{ \sum_{n\in C} \left[\left(\frac{\mathcal{P}^i_{sn} P^j_{nr} P^k_{rs}}{E_{ns} - 2E_{rs}} + \frac{P^j_{sn} \mathcal{P}^i_{nr} P^k_{rs}}{E_{ns} + E_{rs}} \right) \delta(E_{rs} - \hbar\omega) - 2 \frac{\mathcal{P}^i_{sn} P^j_{nr} P^k_{rs}}{E_{ns} - 2E_{rs}} \delta(E_{ns} - 2\hbar\omega) \right] - \sum_{m\in V} \left[\left(\frac{\mathcal{P}^i_{mr} P^j_{sm} P^k_{rs}}{E_{rm} - 2E_{rs}} + \frac{P^j_{mr} \mathcal{P}^i_{sm} P^k_{rs}}{E_{rm} + E_{rs}} \right) \delta(E_{rs} - \hbar\omega) - 2 \frac{\mathcal{P}^i_{mr} P^j_{sm} P^k_{rs}}{E_{rm} - 2E_{rs}} \delta(E_{rm} - 2\hbar\omega) \right] \right\}, \quad (3)$$

where $P^i_{s,n}(\vec{k})$ is the matrix element of the i-Cartesian component of the momentum operator ($\vec{P}$) between states s and n, which may be valence (V) or conduction (C) states at point $\vec{k}$ in the 2D Brillouin zone (BZ), A is the sample area, $E_{nr} = E_n(\vec{k}) - E_r(\vec{k})$, $E_n(\vec{k})$ being the one-electron energy. The emission of SH light is described by the modified momentum operator $\vec{\mathcal{P}} = [S(z)\vec{P} + \vec{P}S(z)]/2$, where $S(z)$ is a function of z, being 1 at the front surface and 0 at the back surface, which avoids the spurious destructive interference of SH light generated at the two surfaces of the slab. We remark that the above expression must be symmetrized in the last two indices (jk) in order to comply with the intrinsic permutation symmetry of $\overleftrightarrow{\chi}$. We should also mention that in the calculation of $\overleftrightarrow{\chi}$, the fundamental electric field oscillating at ω, which induces the nonlinear response, is taken inside the surface [10]. Local-field and excitonic effects are neglected throughout.

Finally, we employ the Kramers-Kronig transform to calculate the real part of $\overleftrightarrow{\chi}$. The components of $\overleftrightarrow{\chi}^s$ for the double-domain (100) surface are obtained through $\chi^s_{\perp\perp\perp} = \chi_{zzz}$, $\chi^s_{\perp\parallel\parallel} = (\chi_{zxx} + \chi_{zyy})/2$, and $\chi^s_{\parallel\parallel\perp} = (\chi_{xxz} + \chi_{yyz})/2$, where $\chi_{ijk} = \chi_{ikj}$ are calculated for each of the two single-domain lattices [11].

We consider a slab consisting of N atomic (100) layers. For a given surface morphology, total energy minimization can be performed to find the equilibrium atomic positions, according to the density functional theory within the local density approximation (DFT-LDA), for a $c(4 \times 2)$ supercell [12]. With these coordinates, we calculate the one-electron energies and momentum matrix elements entering Eq. (3) according to the semiempirical tight-binding (SETB) approach described in Ref. [13]. We mention that the criterion for choosing N and N_k [the number of k-points to sum up in Eq. (3)] is a good numerical convergence of the SHG spectra with respect to them; in particular, the results shown below are for $N = 16$ and for $N_k = 64$ special k-points in the irreducible part of the 2D BZ. For $S(z)$ we have used a step function centered at the middle of the slab. Using smoother functions yields the same SHG line shape with only small changes in the absolute magnitude of $\mathcal{R}$.

In Fig. 1 we show $\mathcal{R}_{pp}$ vs the energy of the SH photon for a Si(100) surface with 1 H, 2 H (monohydride phase), and 4 H (ideally terminated dihydride phase) per Si-Si dimer, along with the room temperature experimental data of Ref. [7]. In the second and third cases all dangling bonds are hydrogen saturated, while in the first case one unsaturated dangling bond per surface dimer survives. The E_1 peak is clearly seen at 3.36 eV, and its intensity gets reduced by increasing the number of hydrogens. Below this peak, only the surface with unsaturated dangling bonds shows some structures, indicating that these small peaks come from transitions across dangling-bond-like surface states, which are suppressed by hydrogen saturation. A peak between E_1 and E_2 (4.3 eV) develops as the

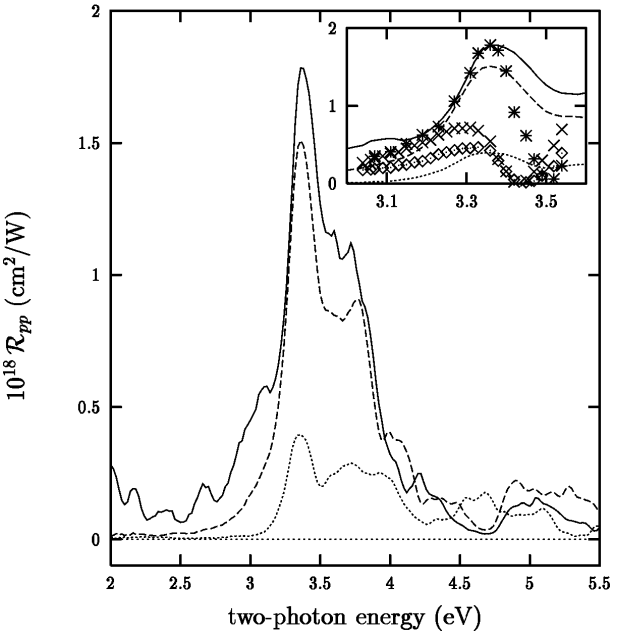

FIG. 1. We show $\mathcal{R}_{pp}$ vs the two-photon energy for the 2×1 Si(100) surface with 1 H (solid line), 2 H (dashed line), and 4 H (dotted line) per Si-Si dimer. From Ref. [7] we also show in the inset the room temperature experimental data for 1 H (stars), monohydride (crosses), and dihydride (rhombi) phase, where the data are rescaled on the vertical axis. The angle of incidence $\theta = 55°$ is the same as in the experiment.

hydrogen coverage increases. For energies above the bulk E_2 transition, the ideally terminated surface shows well developed peaks, whereas for the other two cases the intensity is almost zero. Finally, around 5 eV a structure is present for all of the three surfaces, coincident with the E_1' bulk transition. We mention that these surfaces have 2×1 reconstructions, although the energy minimization had a $c(4 \times 2)$ unit cell as the starting point.

Energy minimization reveals that the most favorable structure for the clean Si(100) surface corresponds to a $c(4 \times 2)$ reconstruction, where the Si-Si dimers alternate in buckling from one neighbor to another in the surface plane [14]. Although RHEED shows a 2×1 unit cell at room temperature, the local structure is $c(4 \times 2)$ [14]. In Fig. 2 we show $\mathcal{R}_{pp}$, for the $c(4 \times 2)$ and 2×1 reconstructed clean Si(100) surfaces, along with the low temperature experimental results from Ref. [7]. The differences between the theoretical peak intensities calculated for the two reconstructions are apparent; however, above E_1 the line shapes show an evident resemblance, whereas for energies below E_1, qualitative differences are present. The three well developed peaks in the $c(4 \times 2)$ spectrum just below E_1 are small shoulders in the 2×1 spectrum. An important observation from the spectrum of the clean and hydrogen-covered surfaces is that several bulk interband transitions known from linear optics, such as E_1', are present and, in contrast with the linear case, show a comparable magnitude with respect to E_1 and E_2. We remark that the intensity of the E_1 peak for the $c(4 \times 2)$ surface is almost a factor of 5 larger than that of the hydrogen-saturated ideal termination, in agreement with experiment.

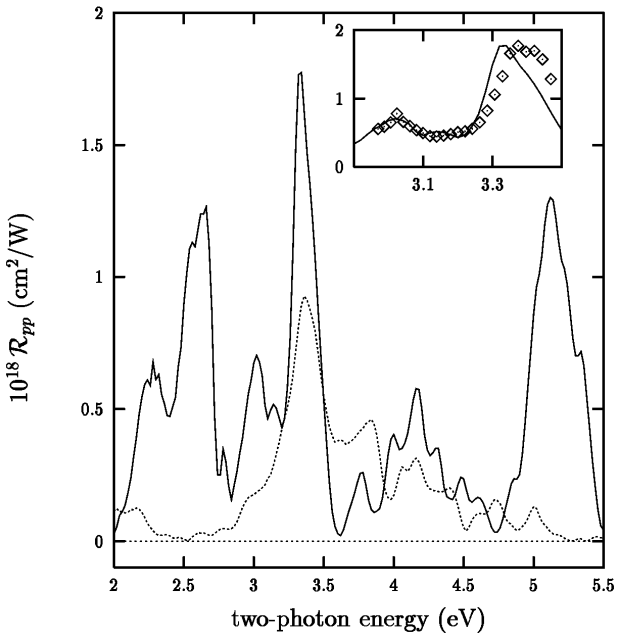

FIG. 2. Same as Fig. 1, for the $c(4 \times 2)$ (solid line) and for the 2×1 (dotted line) reconstructions of the clean Si(100) surface. The inset shows the low-temperature experimental results of Ref. [7] (rhombi, rescaled on the vertical axis), along with the calculated $c(4 \times 2)$ spectrum.

The experimental spectra of Ref. [7] cover only the two-photon energy range from 3 to 3.5 eV, while that of Ref. [6] goes from 2.1 to 3.6 eV. However, the latter shows only a model dependent experimental susceptibility, which makes comparison with our results more subtle; thus we directly compare with the former which shows experimental spectra of $\mathcal{R}_{pp}$. We have shifted upward in energy the theoretical curves by 0.24 eV, in order to have a better correspondence in energy between calculated and measured structures. Differences of this order, often occurring in SETB calculations [15], could be related to surface effects on the electron self-energies. In carrying out the Kramers-Kronig transform, a finite broadening of 25 meV was used; a larger (smaller) broadening will erase (sharpen) some of the small structures. With this broadening the comparison with experiment is quite good. Indeed, for the hydrogen-covered surfaces the position of the E_1 peak and its intensity correlate quite well with the experiments. For the clean surface, we find that the low-temperature experimental spectrum shows, besides the E_1 peak, a peak at 3.02 eV. The calculation carried out for the $c(4 \times 2)$ structure nicely reproduces its line shape; it is present, although weaker, also in the calculated spectra for the clean and partially hydrogenated 2×1 structures, while it disappears after complete hydrogenation. Hence we assign it to transitions across dangling-bond-like surface states. The experiments of Ref. [6] nicely confirm this assignment.

Another important experimental finding is a shift of the E_1 peak as a function of the hydrogen coverage: it redshifts by 0.1 eV in going from the clean surface to the monohydrade phase, and then there is a blueshift of a smaller magnitude when proceeding towards the dihydride phase [7]. Indeed, we find that by including suitable surface localized static electric fields of the order of 10^6 V/cm in the calculations carried out for the various surfaces, the E_1 peak shows the correct experimental behavior. This suggests the presence of built-in electric fields whose strength depends on the hydrogen coverage [16].

The excellent agreement of the present theory with the experimental spectra allows us to answer a very important question: Which components of $\overleftrightarrow{\chi}^s$ are responsible for the observed spectra? To answer, one must be very careful, because of the fact that $\mathcal{R}_{pp}$ depends on $\overleftrightarrow{\chi}^s$ through r_{pp} of Eq. (2), and thus the relevant quantities to analyze are $\overleftrightarrow{\chi}^s$ multiplied by the *radiation* factors, and not the bare susceptibilities alone. Indeed, in Fig. 3 we show the bare susceptibilities and their values multiplied by the corresponding radiation factors [17]. Although the bare $\overleftrightarrow{\chi}^s$ components are all of the same order of magnitude and display structures at similar energy positions, when multiplied by the radiation factors they are substantially modified in their relative magnitude [18]. For this particular surface, we obtain that $\chi^s_{\|\|\perp}$ is mostly responsible for the

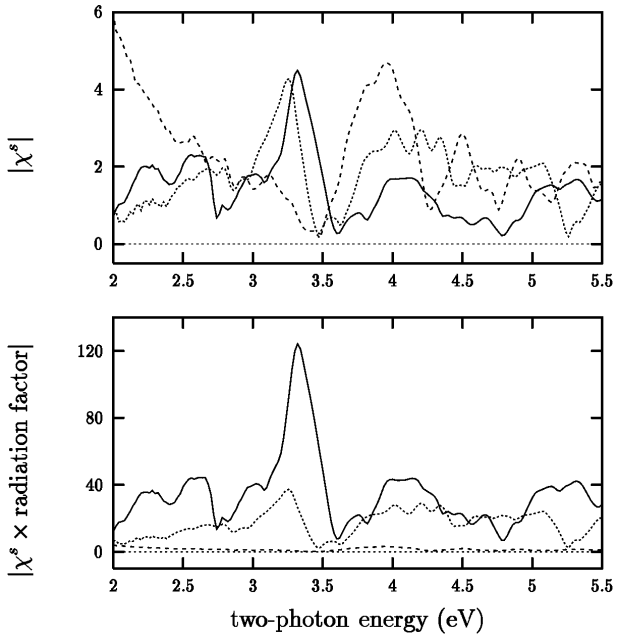

FIG. 3. In the top panel we plot the absolute values of $\chi^s_{\perp\perp\perp}$ (dashed line), $\chi^s_{\perp\parallel\parallel}$ (dotted line), $\chi^s_{\parallel\parallel\perp}$ (solid line) vs the two-photon energy. Likewise, in the bottom panel we plot the same susceptibilities, but multiplied by their corresponding radiation factors given by Eq. (2).

observed spectra, and that the contributions of $\chi^s_{\perp\parallel\parallel}$ and (in particular) of $\chi^s_{\perp\perp\perp}$ are negligible [19]. Also, $\mathcal{R}_{ps}$ is an order of magnitude smaller than $\mathcal{R}_{pp}$, not because $\chi^s_{\perp\parallel\parallel}$ is smaller, but because of the combination of the Fresnel and radiation factors. These conclusions may be altered by local-field effects, which are here neglected. However, the agreement shown here suggests that local-field effects play a minor role in determining SH line shapes.

In summary, we have presented a microscopic calculation of surface SHG which shows an excellent agreement with the experimental spectra of clean and hydrogen-covered Si(100) surfaces. Besides reproducing and explaining the measured resonant peaks in terms of transitions involving bulk or surface states, we conclude that the spectrum of the energetically favorable $c(4 \times 2)$ reconstruction well resembles the experimental one, providing an optical proof of its existence. Also, the behavior of the E_1 peak is related not only to the vertical strain but also to the in-plane reconstruction of the surface. We find structures outside the frequency range investigated so far, which would be very interesting to study experimentally, especially the ones related to surface states, as in Ref. [6], and to the specific bulk transitions, which are difficult to observe in linear optics. With this Letter it is clearly demonstrated that surface SHG is indeed a very fruitful optical spectroscopy.

We thank A. I. Shkrebtii and L. Reining. Also, we thank CONACyT-México (26651-E) and CNR-Italy for partial support. B. S. M. is also grateful for the hospitality of the Department of Physics of the University of Rome "Tor Vergata." The calculations were done on a Cray T3D at CINECA.

*Email address: bms@valkiria.cio.mx
On sabbatical leave at Dipartimento di Fisica, II Università di Roma.

[1] For recent reviews, see Y. R. Shen, Solid State Commun. **102**, 221 (1997); Th. Rasing, J. Magn. Magn. Mater. **175**, 35 (1997); J. E. McGilp, J. Phys. D **29**, 1812 (1996); G. A. Reider and T. F. Heinz, in *Photonic Probes of Surfaces*, edited by P. Halevi (Elsevier, Amsterdam, 1995), p. 413.

[2] W. Daum, H.-J. Krause, U. Reichel, and H. Ibach, Phys. Scr. **T49**, 513 (1993); Phys. Rev. Lett. **71**, 1234 (1993).

[3] B. S. Mendoza and W. L. Mochán, Phys. Rev. B **53**, R10 473 (1996); **55**, 2489 (1997).

[4] K. van Hasselt, Ph.D. thesis, University of Nijmegen, The Netherlands, 1997. A comprehensive list of references for this field is nicely contained.

[5] J. F. McGilp *et al.*, Opt. Eng. **33**, 3895 (1994); C. Meyer *et al.*, Phys. Rev. Lett. **74**, 3001 (1995); J. R. Power *et al.*, *ibid.* **75**, 1138 (1995); K. Pedersen and P. Morgen, Surf. Sci. **377-379**, 393 (1997); P. Godefroy *et al.*, Appl. Phys. Lett. **68**, 1981 (1996).

[6] U. Höfer, Appl. Phys. A **63**, 533–547 (1996).

[7] J. I. Dadap *et al.*, Phys. Rev. B **56**, 13 367 (1997).

[8] Z. Xu *et al.*, J. Vac. Sci. Technol. B **15**, 1059 (1997); O. A. Aktsipetrov *et al.*, Thin Solid Films **294**, 231 (1997).

[9] L. Reining, R. Del Sole, M. Cini, and J. G. Ping, Phys. Rev. B **50**, 8411 (1994).

[10] In particular, these fields are simply given by the external fields properly multiplied by the corresponding Fresnel factors. A more detailed description of the fields, which incorporates the spatial variation of the dielectric function near the surface within the three-layer model [9], shows no change in the SHG peaks' positions, and only a slight difference in their intensity.

[11] Notice that $\chi^{\mathrm{I}}_{zxx} = \chi^{\mathrm{II}}_{zyy}$ and $\chi^{\mathrm{I}}_{xxz} = \chi^{\mathrm{II}}_{yyz}$, for domain I and domain II.

[12] A. I. Shkrebtii (unpublished).

[13] A. Selloni, P. Marsella, and R. Del Sole, Phys. Rev. B **33**, 8885 (1986); P. Vogl, Harold P. Hjalmarson, and John D. Dow, J. Phys. Chem. Solids **44**, 365 (1983).

[14] A. I. Shkrebtii, R. Di Felice, C. M. Bertoni, and R. Del Sole, Phys. Rev. B **51**, 11 201 (1995).

[15] C. Noguez *et al.*, Phys. Rev. Lett. **76**, 4923 (1996).

[16] N. Arzate *et al.* (unpublished).

[17] To obtain $\overleftrightarrow{\chi}^s$ in $\mathrm{m}^2\,\mathrm{V}^{-1}$ units, we must multiply it by $1/n_0 e = 1.11 \times 10^{-19}\ \mathrm{m}^2\,\mathrm{V}^{-1}$, which gives values within the reported numbers of Ref. [4].

[18] For $\hbar\omega$ around 1.6 eV, $k_\perp(\omega)$ is small, while $k_\perp(2\omega)$ is large, since the imaginary part of $\epsilon(2\omega)$ is close to its first peak, occurring at 3.4 eV (i.e., E_1).

[19] Because of the small values of the optical field components $E_\perp$, one can argue that the contribution of $\chi^s_{\perp\perp\perp}$ to the radiated efficiency is effectively small.